ROYAL SOCIETY
OF CHEMISTRY

PAPER

Check for updates

Porphyrin-coated gold nanoparticles associated with X-rays and proton therapy in the treatment of triple-negative breast cancer

Camila Ramos Silva, [iD] ab Guillaume Berionni, [iD] c Martha Simões Ribeiro [iD] b and Anne-Catherine Heuskin*a

Triple negative breast cancer (TNBC) is an aggressive subtype of breast cancer, known for its marked resistance to radiotherapy. Recent research has focused on developing innovative therapeutic strategies to overcome this challenge, with one promising approach being the combination of photodynamic therapy (PDT) and radiotherapy (RT). However, the potential of nanoparticles loaded with photosensitizers to enhance therapeutic efficacy, particularly in combination with charged particle therapies, such as proton therapy (PT), remains underexplored. In this study, we developed porphyrin-coated gold nanoparticles (AuNPs@TMPyP) to integrate PDT with RT using both photons and protons. PDT was performed using AuNPs@TMPyP (35 µg mL^{-1} gold content and 25 µM TMPyP) activated by a red laser (fluence: 40 J cm^{-2}) and combined with either X-rays (225 kVp) or PT (10 keV µm^{-1}). The combined treatment was evaluated for its effects on singlet oxygen generation, reactive oxygen species (ROS) production, mitochondrial membrane potential, and cell death pathways. Additionally, we assessed the survival fraction of both healthy and tumor breast cells. A 3D spheroid model was employed to further investigate the efficacy of the AuNPs@TMPyP-mediated PDT in combination with RT. Intracellular uptake of AuNPs@TMPyP significantly impaired antioxidant defenses, through reduction of thioredoxin reductase levels. Under combined treatment, we observed increased ROS production, reduced survival fraction, and loss of mitochondrial membrane potential, along with increased apoptosis. Our findings suggest that AuNPs@TMPyP-mediated PDT significantly enhances radiosensitization and amplifies the therapeutic response when combined with either X-rays or PT, while exhibiting selectivity toward tumor cells, positioning it as a promising strategy for treating TNBC.

Introduction

Triple-negative breast cancer (TNBC) is a biological subtype of breast cancer, representing 15–20% of all breast cancers cases. It is characterized by the absence of estrogen and progesterone receptors, as well as the human epidermal growth factor receptor 2. These characteristics make TNBC an aggressive form of breast cancer with a poor prognosis and an average survival time of 18 months.[1] Additionally, TNBC tends to grow and spread more rapidly, often leading to distant metastases in the lungs and brain, which complicates disease management.[2]

The treatment of TNBC remains limited, as it is not responsive to conventional treatments, such as adjuvant radiotherapy (RT), which is traditionally administered following mastectomy or conservative breast surgery to induce DNA

damage in remaining cancer cells and halt their reproduction.[3] Consequently, a prolonged treatment period and cumulative doses of ionizing radiation (IR) are often required, leading to several side effects and cardiac disease, mainly due to the deposition of high doses in organs at risk (OAR).[4,5]

Over the last few decades, charged particles such as protons (H$^+$) have been increasingly used as an alternative to achieve high conformality, avoiding the deposition of dose in surrounding healthy tissue and minimizing high doses in the OAR.[6] In proton therapy (PT/H$^+$), it is possible to concentrate the dose in the tumor by modulating the position of the Bragg peak within the target volume, thereby reducing the dose absorbed by surrounding tissues by approximately 60% compared to conventional RT.[7] Like X-ray, protons promote DNA ionization both indirectly through reactive oxygen species (ROS) production and directly, resulting in more complex DNA damage.[8] Although, PT has not been the most widely used form of IR, particularly in breast cancer, it is currently indicated for selected cases of early-stage and locally advanced disease.[9,10] However, despite the advantages of PT, including its favourable

aNamur Research Institute for Life Sciences (NARILIS) – University of Namur, Namur, Belgium. E-mail: anne-catherine.heuskin@unamur.be

bCenter for Lasers and Applications, Energy and Nuclear Research Institute-IPEN-CNEN, São Paulo, Brazil

cChemistry Department-University of Namur, Namur, Belgium

depth-dose profile, overcoming radioresistance remains a significant challenge.[11]

Photodynamic therapy (PDT) is a promising cancer treatment due to its tumor selectivity, low side effects and cost-effectiveness.[12,13] PDT involves the use of a photosensitizer (PS) along with a resonant wavelength that culminates in the formation of ROS leading to cell death. However, the challenges of delivering the PS to deep-seated tumors and mainly the shallow penetration of light through tissue to activate the PS have hindered the widespread use of PDT in oncology.[14] These limitations complicate the assessment of its real effects as standalone therapy or in association with regular therapies, such as RT.[15,16]

With the advance of nanomedicine, gold nanoparticles (AuNPs) have been studied to enhance the effects of the RT due to their ability to increase dose deposition in the target volume as well as ROS production.[17] Some studies have evidenced increased oxidative stress and reduced mitochondrial membrane potential in cells pre-incubated with AuNPs.[18,19] Additionally, AuNPs conjugated with PS with or without specific tumor targeting have also been used in PDT and improved the homogeneity of PS distribution within the tumor.[20] Thus, AuNPs coated with PS to enable a multifaceted treatment, surpassing the challenges of each standalone therapy, would be a promising therapeutic strategy.

Here, we combined PDT mediated by porphyrin-coated AuNPs (AuNPs@TMPyP) with either X-rays or PT as a novel strategy to enhance cancer treatment. Using MDA-MB-231 cells to model TNBC to verify the effects of the treatment, we established PDT and RT protocols and assessed surviving fraction, ROS generation, mitochondrial membrane potential, and cell death pathways. We also evaluated the impact of treatments on 3D TNBC spheroids viability and verified the effects on the survival fraction in MCF10A as healthy breast tissue. Our findings indicate that this multifaceted approach may be a promising therapeutic strategy for TNBC, capable of disrupting thioredoxin reductase activity and enhancing long-term tumor control.

Material and methods

This study comprised four experimental groups: control, AuNPs, AuNPs@TMPyP and TMPyP, each subjected to four treatment conditions: (i) unexposed, (ii) laser irradiation, (iii) X-rays or H$^+$ irradiation and (iv) combined treatment with laser plus X-rays or H$^+$

AuNPs synthesis, functionalization and characterization

AuNPs were synthesized using the reverse Turkevich method to achieve a 15 nm diameter.[21] Sodium citrate (pH = 7.5, 5.3 mM-Merck, Belgium) was heated at 100 °C, and HAuCl$_4\cdot$3H$_2$O (pH = 1.6, 25.4 mM-Merck, Belgium) was added once bubbles appeared, stirring until it turned red. Coating by ligand exchange was performed at room temperature with LA-PEG$_{1k}$-COOH (lipoic acid poly (ethylene glycol), 10 mM-BiopharmaPEG, USA), stirred overnight. The mixture was then purified using a 10 kDa molecular weight cut-off membrane filter (Amicon® ultra centrifugal filter-Merck, Belgium) until the conductivity reached approximately 1 μS cm^{-1}.

Next, TMPyP (5,10,15,20-tetrakis(1-methyl-4-pyridinio) porphyrin tetra (p-toluenesulfonate), Merck, Belgium) was added to AuNPs (1 : 4 (v/v)), mixed overnight, and purified to remove excess reagents, reaching similar conductivity to the pegylated AuNPs. AuNPs@TMPyP were lyophilized through freeze-drying system and kept at 4 °C in dark conditions.

The hydrodynamic diameter and the zeta potential (ζ) of AuNPs@TMPyP were determined by dynamic light scattering (Zetasizer advance ranger-Malvern Panalytical, UK) through three different dispersion media: water, Dulbecco's Modified Eagle's Medium (DMEM-Merck, Belgium) and DMEM supplemented with 10% fetal bovine serum (FBS-Gibco, Belgium). Particle size was assessed using transmission electron microscopy (TEM) on a Philips Tecnai 10 microscope at 100 KeV in bright-field mode. Drops of AuNPs and AuNPs@TMPyP were deposited onto carbon-coated Cu grids to acquire TEM images. The analysis was conducted using the NanoDefine plugin from ImageJ® (ImageJ 1.53T, 64-bit). AuNPs@TMPyP were further characterized by Fourier transform infrared spectroscopy (FTIR; Spectrum Two, PerkinElmer, USA) to confirm the presence of the TMPyP coating. Spectra were recorded in the range of 4000 to 500 cm^{-1}.

Gold concentration in AuNPs@TMPyP solutions was determined using atomic absorption spectroscopy (AAS-7000 F, Shimadzu, Japan) with a standard calibration curve. The gold plasmon band was monitored by UV-vis spectroscopy (400–800 nm) using a Spectramax M4 microplate reader (Molecular Devices, USA) using the same dispersion media described above at two different experimental time points: 0 and 24-h. TMPyP concentration was measured spectrophotometrically using its molar extinction coefficient at the Soret band ($\varepsilon_{420\ nm}$ = 220 000 cm^{-1} M^{-1}).[22] Emission spectra were recorded for all experimental groups under identical conditions, with excitation at 420 nm and emission at 660 nm.

Cell culture

MDA-MB-231 cells (ATCC HTB-26) were selected as the TNBC model in this study, as they are the most widely used in the literature for this cancer subtype, owing to their reproducibility, high aggressiveness, and adaptability to both 2D and 3D culture systems[23] Cells were cultured in DMEM supplemented with 10% FBS, 100 U mL^{-1} penicillin, and 100 μg mL^{-1} streptomycin (Merck, Belgium). MCF10A cells (ATCC CRL-10317) were grown in DMEM/F-12 (Merck, Belgium) with special supplementation: 5% horse serum (Invitrogen, Belgium), human epidermal growth factor (20 ng mL^{-1}, Protech, UK), hydrocortisone (0.5 mg mL^{-1}, Merck, Belgium), cholera toxin (100 ng mL^{-1}, Merck, Belgium) and insulin (10 μg mL^{-1}, Merck, Belgium). Both cell lineages were kept at 37 °C in a humidified atmosphere with 5% CO$_2$.

For 3D cell culture, 3×10^2 MDA-MB-231 cells in 100 μL were added to Nunclon™ Sphera plates (ThermoFisher Scientific, Belgium), centrifuged at 150 g for 10 min, and maintained

under culture conditions for 120 h. The maximum diameter allowed for spheroids was 200 μm at the start of experiment to guarantee shoot-through proton irradiation.

AuNPs@TMPyP internalization and localization

Under experimental conditions the gold concentration used was approximately 35 μg mL^{-1}, corresponding to 25 μM of TMPyP. This porphyrin concentration was fixed, and the gold concentration was adjusted accordingly.[15] To assess the intracellular content of gold, MDA-MB-231 and MCF10A cells were cultured in flask of 75 cm^2 and incubated with AuNPs@TMPyP for 24 h. Then, cells were detached, washed twice with medium, centrifuged and counted. The pellets were digested using 2 mL of aqua regia (37% HCl, 65% HNO$_3$-Merck, Belgium) for 7 days. The Au content was quantified using AAS and a known calibrated curve of gold standard solution diluted in *Acqua regia* (Merck, Belgium).

To evaluate TMPyP content, a total of 10 000 cells were seeded into 96-well plate, followed by the addition of AuNPs@TMPyP for 24 h. Subsequently, the cells were washed again, and phosphate-buffered saline (PBS-Merck, Belgium) was added to each well. Fluorescence intensity was then measured for all conditions using a spectrophotometer (Spectramax M4, MolecularDevices, USA), with excitation and emission wavelengths at 420 nm and 660 nm, respectively.

For localization within MDA-MB-231 cells, a specific protocol for cell fixation (2.5% glutaraldehyde and 0.1% cacodylate) and progressive dehydration with ethanol was followed. After this process, cells embedded in a mixture of propylene oxide and resin were sliced and mounted on carbon-coated Cu grids to acquire TEM images (Philips Tecnai 10, 100 KeV).[24] Images were captured in all experimental conditions at different magnification to detect AuNPs@TMPyP.

Thioredoxin reductase (TrxR)

To assess the redox status of the cells, the enzymatic activity of TrxR was quantified using a commercial kit (Sigma-Aldrich, Belgium). After 24 h of AuNPs incubation, cells were detached, centrifuged, and resuspended in a homemade lysis solution (9% sucrose, 5% aprotinin (Merck, Belgium) in deionized water, v/v) for 30 min. Subsequently, a freeze-thaw process was performed to ensure complete cell disruption. The reduction of Ellman's reagent by NADPH to thionitrobenzoic acid was then monitored by measuring the absorbance at 412 nm over a 10-min period using a spectrophotometer (SpectramaxM4, Molecular Devices, USA).

Photodynamic therapy

PDT was aimed to be used as a priming for RT, thus, cells were seeded 48 h before treatment. The culture medium was replaced with 35 μg mL^{-1} of AuNPs, AuNPs@TMPyP, or TMPyP (25 μM), diluted in culture medium, and incubated for 24 h. Cells were then irradiated with a red laser ($\lambda = 660$ nm, 100 mW, 0.1 cm^2, DMC, Brazil) at an energy of 4 J and fluence of 40 J cm^{-2}. The laser tip was positioned at the bottom of the culture plate to standardize irradiation.

Radiotherapy

RT was performed immediately after PDT. A dose of 2 Gy, which results in a 20% reduction in cell viability for X-rays, was selected (Fig. SM1).

X-ray radiation. Cells were irradiated with a homogeneous X-ray beam from an X-Rad 225 XL (PXi Precision X-ray, CT, USA) at 225 kVp, 13.5 mA, and a fixed dose rate of 2 Gy min^{-1}. After exposure, the medium was removed, cells were washed, fresh medium was added, and cells were incubated until further analysis. The same protocol was applied for 3D cell cultures.

Proton irradiation. Homemade irradiation chambers were used for PT, as previously described.[25] Briefly, the surface of the chambers (Mylar foil of 3 μm thickness) was sterilized and treated with a droplet (40 μL, 0.1 μg mL^{-1}) of fibronectin (Gibco, USA) 48 h before irradiation. Then, the cells (2×10^4) were seeded in the center of chambers, which were closed with a plastic cap to avoid dehydration. Two hours after seeding, the chambers were filled with culture media. The media was replaced to fresh media with AuNPs@TMPyP 24 h before irradiation.

Irradiation was performed using a homogenous proton beam over 1 cm^2, produced by a 2-MV Tandem accelerator (High Voltage Engineering Europa, Netherlands). The detailed irradiation protocol and accelerator set up were previously reported.[26] In summary, pristine proton peaks were extracted in air through a 1-μm silicon nitride window and the irradiation chambers were placed on a sample holder fixed at the end of the beamline. Homogeneity was checked each millimeter over 1 cm^2 with a passivated implanted planar silicon detector moved along the x and y directions (perpendicular to the beam). The dose rate (fixed at 2 Gy min^{-1}) was also assessed every millimeter and errors were less than 5% in the cell sample region. The linear energy transfer (LET) at the cell sample location was computed with the stopping and range of ions in matter (SRIM) software and reached 10 keV μm^{-1}.[25]

After the irradiation, the medium was discarded and cells were washed with PBS. A sterile cotton swab was used to take any cells that might have diffused outside the irradiated area. Irradiated cells were then detached using trypsin 0.25% and seeded again in plates for further analysis.

To conduct 3D irradiation, spheroids were seeded 6-h before irradiation in the chambers. After irradiation, they were detached with a pipette and transferred to NunclonTM Sphera plates (ThermoFisher Scientific, Belgium).

Clonogenic assay. Immediately after treatments, cells were detached using trypsin 0.25% (Invitrogen, Belgium), counted, and seeded in 6 well plates at different concentrations to obtain countable colony numbers. These cells were maintained at 37 °C in 5% CO$_2$ for 14 days and then the colonies were stained with a solution of 2% violet crystal in ethanol. The number of visible colonies (containing 50 or more cells) were counted manually. The plating efficiency (PE) was calculated by dividing the number of colonies by the initial numbers of seeded cells. The surviving fraction was obtained by the PE ratio for treated cells to the PE of control group (unexposed). To assess the ability of AuNPs@TMPyP to enhance cell death, the amplification factor

(AF) was calculated relative to the dose of 2 Gy.[18] Combination drug interaction (CDI) was also calculated as reported in.[27]

$$AF[\%] = \left[\frac{SF_{IR} - SF_{CT}}{SF_{IR}}\right] \times 100 \qquad (1)$$

where: SF_{IR} = survival fraction of irradiated control (X-rays or H^{+}); SF_{CT} = survival fraction of combined treatment (AuNPs, AuNPs@TMPyP and laser).

ROS and singlet oxygen production

Three hours post-treatment, ROS levels were evaluated using 20 µM of 2′, 7′-dichlorofluorescin diacetate (H$_2$DCFHDA-Merck, USA) in 1×10^4 cells. Following 45 min of incubation, green fluorescence was measured using a spectrophotometer (SpectraMax M4, USA) with excitation and emission wavelengths of 485 and 535 nm, respectively. This specific experimental timing was adapted to our setup, as detaching and reseeding the cells after H^{+} exposure required additional time.

The generation of $^1O_2$ was measured using the sensor green singlet oxygen kit (SOSG-ThermoFisher Scientific, USA). Briefly, a solution of SOSG (2 µM) was added to the experimental groups before the treatment. The fluorescence intensity was read immediately after treatments using a spectrophotometer with excitation and emission wavelengths of 504 and 525 nm, respectively. For both assays, the data were normalized to the control.

Mitochondrial membrane potential ($\Delta\Psi$)

Twenty-four hours after treatments, the $\Delta\Psi$ was assessed in all experimental groups through Cell Meter™ JC-10 MMP assay kit (AAT Bioquest, USA). Cells were washed with PBS and 50 µL of JC-10 dye-loading solution was incubated for 40 min under culture conditions. Fluorescence at two wavelengths (excitation 490/540 nm and emission 525/590 nm, respectively) was measured. In polarized healthy mitochondria (high $\Delta\Psi$), JC-10 forms aggregates that emit orange fluorescence (~590 nm), whereas in depolarized mitochondria (low $\Delta\Psi$), it remains in its monomeric form, emitting green fluorescence (~525 nm).

Cell death pathways. The percentage of early apoptotic cells (PI[−]/Annexin V[+]) and late apoptotic/necrotic cells (PI[+]/Annexin V[+]) were evaluated 24 h post-treatment for all experimental conditions. Cells were detached, washed, and stained with propidium iodide (PI, 1 mg mL^{−1}-Sigma-Aldrich, USA) and 5 µL of Annexin V conjugated with Alexa fluor 647 (ThermoFisher Scientific, USA). Fluorescence intensity was recorded using a flow cytometer (FACS verse-BD, USA) with 10 000 events per experimental group.

3D spheroid viability. After treatments, spheroids were monitored for 21 days and cell viability was measured using the CellTiter-Glo® 3D Cell Viability Assay (Promega, USA).

Statistical analysis. The data distribution for each assay was verified by the Shapiro–Wilk test with the OriginPro 2018 program. Group comparisons were conducted using One or Two-way ANOVA (factors: group and treatment), with Fisher LSD as a post-test. All experiments were repeated at least three times on three different days and data are presented as means ± standard error of the mean (SEM). Statistically significant differences were considered when $p < 0.05$.

Results

AuNPs synthesis, characterization and cellular impact

The porphyrin coating did not modify the general shape of AuNPs, as TEM images (Fig. 1a and b) showed spherical AuNPs in both conditions, with an average diameter of 17.80 ± 3.90 nm and 17.70 ± 3.32 nm, respectively (Fig. 1c and d). In contrast, the ζ-potential varied as a function of dispersion medium and experimental time for both nanoparticle formulations (Fig. 1e). Notably, the DMEM + 10% FBS dispersion medium, which was used throughout the biological experiments, maintained greater colloidal stability over time regardless of porphyrin functionalization. Conversely, the hydrodynamic diameter in this dispersion medium exhibited a significant increase over time for AuNPs but an opposite behavior for AuNPs@TMPyP.

FTIR analysis confirmed TMPyP binding to AuNPs, as evidenced by a vibrational band around 1641 cm^{−1} in both TMPyP and AuNPs@TMPyP spectra (Fig. 1f), corresponding to the C=N stretching vibration of the pyridyl rings.[28] UV-vis absorption (plain lines, Fig. 1g) using water as dispersion media at 0 h revealed a peak around 425 nm for both TMPyP porphyrin and AuNPs@TMPyP, while the plasmon resonance band for AuNPs was observed at 525 nm. Emission peaks at 660 nm and 720 nm were observed for AuNPs@TMPyP, while TMPyP showed a peak at 720 nm with a shoulder at 680 nm (dashed lines, Fig. 1g). Following 24 h of incubation in water, a difference in absorption intensity around 520 nm was observed between TMPyP and AuNPs@TMPyP, with the latter exhibiting higher intensity (Fig. 1i). Regarding fluorescence emission, changes in intensity at the emission peaks at 660 nm and 720 nm were observed for all porphyrin-containing groups compared with 0 h. When dispersed in DMEM supplemented with 10% FBS, a reduction in absorbance at 425 nm was detected for AuNPs@TMPyP, accompanied by an increase in intensity around 560 nm for all TMPyP-containing formulations and a narrowing of the plasmon band for AuNPs (Fig. 1h). In the emission spectra, a high intensity peak at 660 nm was observed for both porphyrin groups under these conditions. Following 24-h of incubation, an absorption band shift toward approximately 560 nm was more evident for all experimental groups (Fig. 1j). The emission spectra at this time point were predominantly centred around 660 nm.

After 24 h of incubation, the intracellular gold concentration was comparable for AuNPs and AuNPs@TMPyP within each cell line, indicating that porphyrin functionalization did not affect gold internalization (Fig. 2a). In contrast, a statistically significant difference was observed between the tumor and non-tumorigenic cell lines, with higher gold accumulation in cancer cells. Similarly, gold conjugation did not influence porphyrin uptake, as fluorescence emission was comparable between AuNPs@TMPyP and free TMPyP (Fig. 2b). This behavior was observed in both cell lines; however, fluorescence intensity was markedly higher in tumor cells than in MCF10A
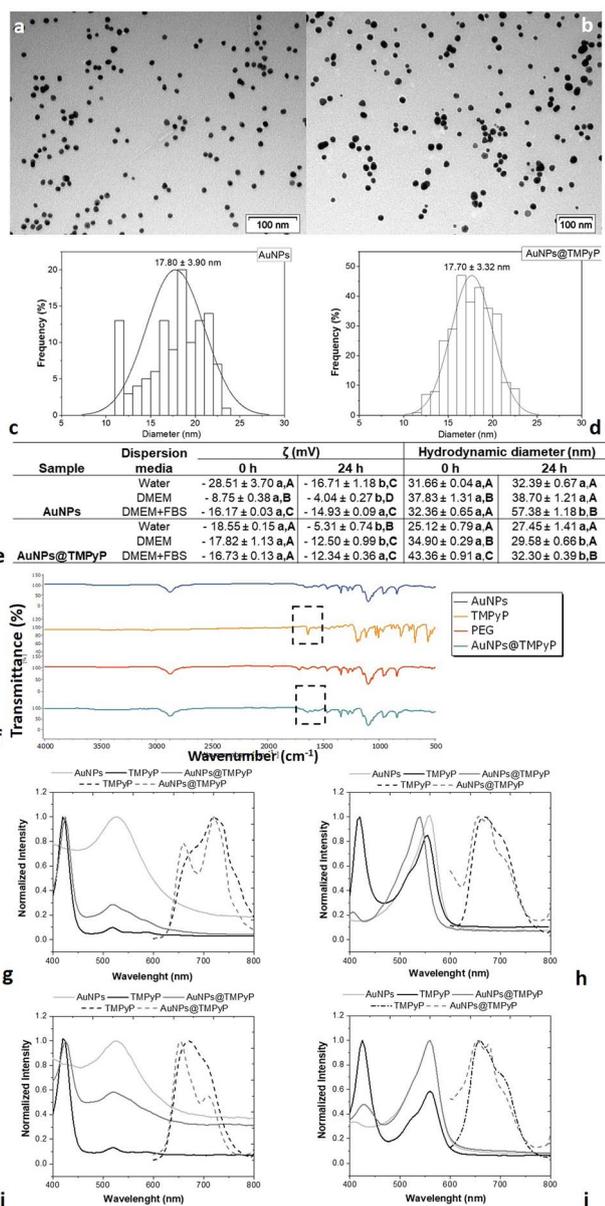
Fig. 1 TEM images of (a) AuNPs and (b) AuNPs@TMPyP (scale bar: 100 nm); frequency of distribution ± standard deviation of (c) AuNPs and (d) AuNPs@TMPyP; (e) Zeta potential and hydrodynamic diameter at 0 and 24-h in different dispersion media: water, DMEM and DMEM supplemented with 10% FBS; (f) FITR spectra. The highlighted region shows a similar peak around 1641 cm^{-1} for AuNPs@TMPyP and TMPyP; absorbance (plain lines) and emission spectra (dashed lines) using water as dispersion solution at 0-h (g) and 24-h (i); absorbance (plain lines) and emission spectra (dashed lines) using DMEM supplemented with 10% FBS as dispersion solution after 0-h (h) and 24-h of insertion (j). Different lowercase letters indicate statistically significant differences over time within the same dispersion medium, whereas uppercase letters denote statistically significant differences among experimental groups with the same nanoparticle.
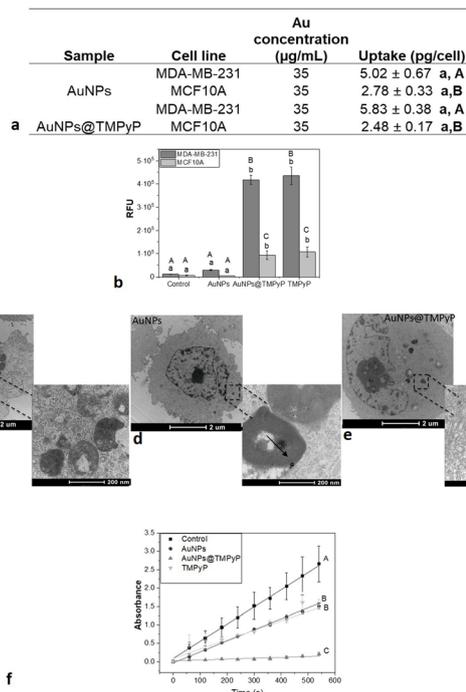

Fig. 2 (a) Gold uptake by MDA-MB231 and MCF10A cells measured by AAS; (b) relative fluorescence indicating porphyrin internalization for MDA-MB-231 and MCF10A cells; (c, d and e) TEM images of MDA-MB-231 cells, with arrows indicating AuNP localization; (f) TrxR activity measured kinetically over 10 min (as absorbance at 412 nm μg^{-1} of protein). Different capital letters indicate statistically significant differences between cell type, while lowercase letters represent comparisons among experimental groups considering the same cell line.

vesicles. No free AuNPs were detected in the cytoplasm or nucleus, and both AuNPs and AuNPs@TMPyP exhibited similar intracellular localization patterns.

Regarding the cellular redox homeostasis, control cells exhibited the highest TrxR activity, whereas both AuNP and TMPyP-treated cells showed comparable reductions. Notably, AuNPs@TMPyP produced the most pronounced reduction in TrxR activity of breast tumor cells over time (Fig. 2f).

Mechanistic insights and surviving fraction analysis of AuNPs@TMPyP under irradiation

AuNPs@TMPyP group at laser exposure showed the highest level of $^1O_2$ and TMPyP group showed higher levels than AuNPs group. However, this effect was not observed under X-ray or laser + X-rays irradiation, where similar $^1O_2$ were detected across between the groups with TMPyP (Fig. 3a).

On the other hand, no statistically significant differences in ROS production were observed among groups exposed to laser irradiation alone. However, under X-ray exposure, the control and AuNPs@TMPyP groups showed the highest ROS levels. In the laser + X-rays condition, no significant differences were detected between groups. Additionally, the AuNPs@TMPyP group irradiated with X-rays and laser + X-rays exhibited approximately 2.0 and 1.5-fold increases, respectively, in ROS
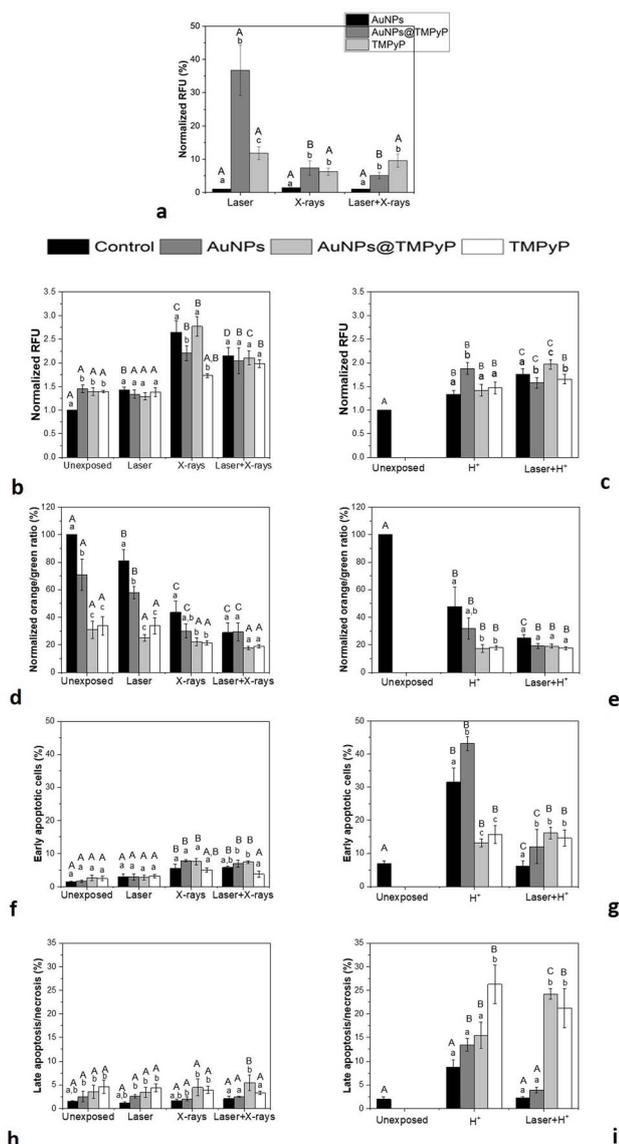
cells, reflecting the greater porphyrin internalization by cancer cells relative to healthy epithelial cells.

TEM imaging revealed no AuNPs in the control group (Fig. 2c), whereas both AuNPs (Fig. 2d) and AuNPs@TMPyP (Fig. 2e) were observed within intracellular membrane-bound

Fig. 3 (a) Singlet oxygen measurements immediately after irradiation. ROS levels following 3 hours for (b) X-ray and (c) H$^+$ irradiation. Normalized orange/green ratio of $\Delta\Psi$ after 24 h of (d) X-ray and (e) H$^+$ irradiation. Cell death pathways: early apoptosis after 24 h of (f) X-ray and (g) H$^+$ irradiation; late apoptosis/necrosis 24 h after (h) X-ray and (i) H$^+$ irradiation. Capital letters indicate statistically significant differences between irradiation conditions within each experimental group, while lowercase letters represent comparisons among experimental groups under the same irradiation condition. AuNPs, AuNPs@TMPyP and TMPyP groups under exposed condition are the same for both radiation modalities.

levels compared to the unexposed and laser conditions. Indeed, ROS levels in the AuNPs@TMPyP group decreased by approximately 0.75-fold under laser + X-rays compared to X-rays alone (Fig. 3b).

Concerning PT, a statistically significant increase in ROS levels was observed for the AuNPs group compared to the other conditions. In contrast, the AuNPs@TMPyP group showed a similar increase only under laser + H$^+$ irradiation, while the

TMPyP group did not exhibit statistically significant differences under any irradiation condition (Fig. 3c). Interestingly, ROS levels induced by PT were considerably lower than those observed with X-rays across all experimental groups.

Both AuNPs@TMPyP and TMPyP treatments produced similarly reduced $\Delta\Psi$ compared with control and AuNP-only groups, regardless of irradiation source. In control and AuNP-treated cells, exposure to X-rays or combined laser + X-rays caused a marked $\Delta\Psi$ decrease relative to laser and to unexposed cells (Fig. 3d). PT also induced a statistically significant $\Delta\Psi$ reduction versus unexposed cells. Moreover, under laser + H$^+$ exposure, control cells showed a further significant drop in $\Delta\Psi$ (from $47.84 \pm 14.02\%$ down to $24.94 \pm 2.50\%$) (Fig. 3e). X-ray and H$^+$ exposures yielded comparable levels of $\Delta\Psi$ depolarization.

When assessing early apoptosis, no statistically significant differences were observed among groups for any irradiation condition, except that AuNPs@TMPyP showed more apoptotic cells (around 1.9 times) than TMPyP group under combined laser + X-ray exposure. On the other hand, X-ray or combined laser + X-ray exposure significantly elevated apoptosis levels across all groups (Fig. 3f). Under H$^+$ irradiation, both AuNPs@TMPyP and TMPyP groups exhibited significantly fewer early apoptotic cells than the control and AuNPs groups, and this reduction was sustained under combined laser + H$^+$ exposure. Additionally, laser + H$^+$ irradiations led to a significantly greater decrease in early apoptosis compared to H$^+$ alone in the control and AuNPs groups (Fig. 3g). As expected, the percentage of cells undergoing early apoptosis was higher following PT compared to X-ray exposure, regardless of the experimental group.

Late apoptosis and necrosis were considered together due to compromised membrane integrity. The experimental groups were generally similar across treatment modalities, except in the first two, where TMPyP group had higher levels than the control group. The AuNPs@TMPyP group showed increased levels of late apoptosis/necrosis in relation to the control under X-rays exposure, and this effect was significantly greater under laser + X-rays (Fig. 3h).

Under H$^+$ irradiation, only the TMPyP group exhibited a statistically significant increase in late apoptosis (Fig. 3i). Following laser + H$^+$ exposure, the AuNPs@TMPyP group also showed significantly elevated levels, comparable to the TMPyP group. Once again, PT induced higher levels of late apoptotic cells than X-rays, regardless of the treatment group.

The radiosensitizing effects of treatments were further evaluated based on the survival fraction and all experimental groups showed statistically significant difference compared to unexposed control (Fig. 4a). This trend was maintained for the other experimental modalities and AuNPs@TMPyP group was statistically significant different of TMPyP group in these conditions. Interestingly, under laser + X-rays modality, AuNPs@TMPyP exhibited the lowest surviving fraction (0.14 ± 0.005) compared to the other experimental group ($\sim80\%$ and 42% comparing with control and TMPyP groups, respectively). All the groups exhibited differences between the modalities,
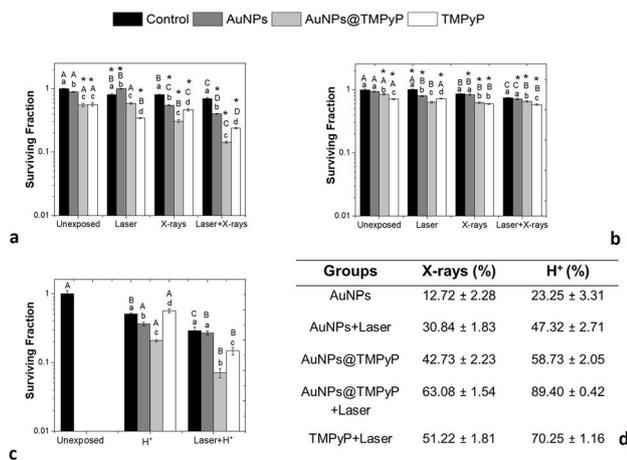
Groups	X-rays (%)	H⁺ (%)
AuNPs	12.72 ± 2.28	23.25 ± 3.31
AuNPs+Laser	30.84 ± 1.83	47.32 ± 2.71
AuNPs@TMPyP	42.73 ± 2.23	58.73 ± 2.05
AuNPs@TMPyP +Laser	63.08 ± 1.54	89.40 ± 0.42
TMPyP+Laser	51.22 ± 1.81	70.25 ± 1.16

Fig. 4 Survival fraction 14 days following treatment for (a) MDA-MB-231 and (b) MCF10A cells exposed to X-rays; (c) MDA-MB-231 cells submitted to H⁺ and (d) amplification factor at 2 Gy for MDA-MB-231 cells. Capital letters indicate statistically significant differences between irradiation conditions within each experimental group, while lowercase letters represent comparisons among experimental groups under the same irradiation condition. The asterisk represents statistically significant difference between cell lines within the same experimental group.

with laser + X-rays displaying the most enhanced therapeutic outcomes.

MCF10A cells, used as a healthy cells model (Fig. 4b) showed statistically significant difference between groups with TMPyP (free or loaded on AuNPs) under unexposed condition and this behavior was similar under other modalities. However, under X-rays modality this trend was different, as these experimental groups were similar and statistically different from control and AuNPs, respectively. Curiously, the surviving fraction for AuNPs@TMPyP group was not influenced by the addition of X-rays to the treatment modality. In general, it was possible to identify that the treatments were more effective for MDA-MB-231 cells, as differences were denoted between the cell lines under different groups and conditions.

Under H⁺ irradiation (Fig. 4c) all the groups presented statistically significant differences, with AuNPs@TMPyP group displaying the lower survival fraction. Under laser + H⁺ condition, this trend was maintained, expect for AuNPs group which was similar to control group. The modalities influenced the results for each experimental group, showing better results for laser + H⁺. Overall, a ~40% difference in survival fraction was noted between X-rays and H⁺ for similar groups.

The amplification factor was calculated to assess the sensitization effects of AuNPs and TMPyP (free or loaded on AuNPs) in relation to X-rays or H⁺ at a dose of 2 Gy (Fig. 4d). Notably, all groups showed enhanced results compared to radiation alone, with AuNPs@TMPyP displaying the highest values.

CDI was also calculated to evaluate the interaction between AuNPs@TMPyP-mediated PDT and both X-rays and H⁺ irradiation. CDI values were below 1 for both modalities ($CDI_{X-rays} = 0.83$ and $CDI_{H^+} = 0.46$), indicating a synergistic effect.

Effects of the treatments on a 3D spheroid model of TNBC

Spheroids were treated, monitored over 21 days (Fig. 5a and c) and spheroid viability was assessed. Under laser exposure, only the spheroids treated with AuNPs showed significantly higher viability compared to other groups (Fig. 5b). Following X-ray irradiation, both AuNPs and AuNPs@TMPyP-treated spheroids exhibited significantly greater viability than the control and TMPyP groups. In contrast, combined laser + X-ray treatment resulted in a marked reduction of luminescence across all
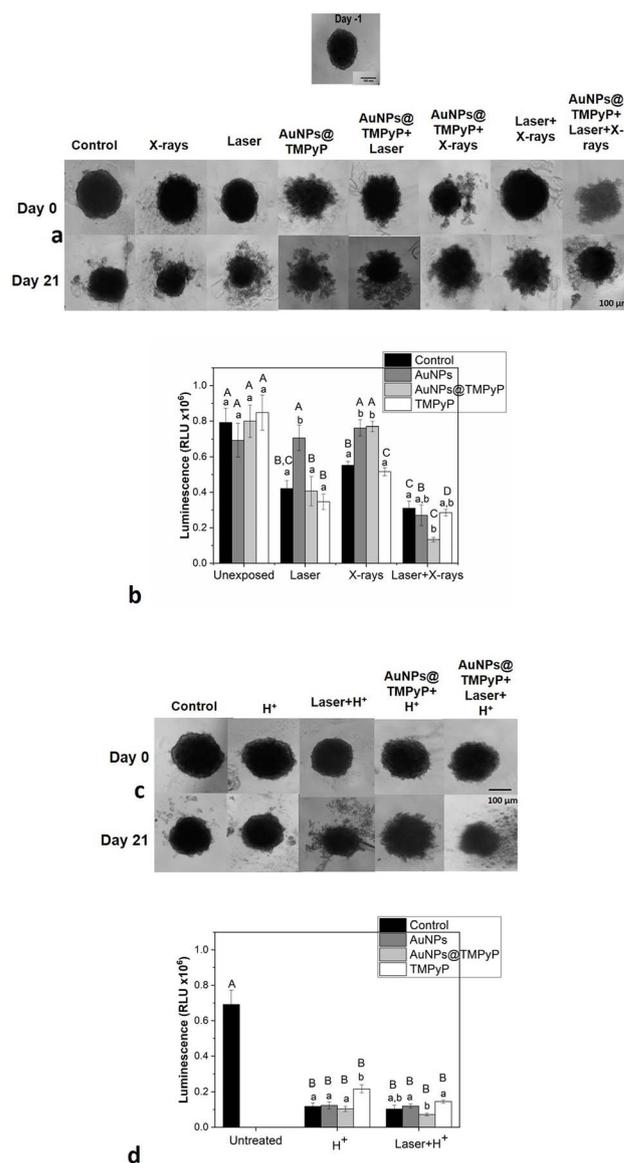

Fig. 5 (a) Representative spheroid photomicrographs for X-ray on days −1 (before IR exposure), 0 (24 h after treatment) and 21; (b) cell viability on day 21 for X-ray radiation; (c) representative spheroid photomicrographs for groups exposed to H⁺ (scale bar: 100 μm) and (d) cell viability on 21st day for groups treated with H⁺. Capital letters indicate statistically significant differences between irradiation conditions within each experimental group, while lowercase letters represent comparisons among experimental groups under the same irradiation condition.

groups, although only the AuNPs@TMPyP group remained significantly different from control. Overall, spheroid viability varied significantly with the type of exposure modality.

Considering PT alone, it effectively reduced cell viability compared to the untreated modality, although the TMPyP group exhibited higher viability than the other irradiated groups (Fig. 5d). In contrast, the AuNPs@TMPyP group showed the lowest viability when combined with laser and H^+ exposures, however not statistically difference in relation with control group at the same conditions was identified.

Discussion

In this work, we synthesized and characterized AuNPs@TMPyP, then combined them with red laser irradiation to assess whether PDT could prime and enhance the efficacy of H^+ and X-ray RT against TNBC. Our results show that AuNPs@TMPyP-mediated PDT enhanced the efficacy of both modalities.

Characterization of AuNPs@TMPyP confirmed effective TMPyP porphyrin coating, as demonstrated by UV-vis spectra, FTIR profiles, and TMPyP fluorescence-based cellular internalization when compared to free TMPyP. A shift in the UV-vis absorption bands was observed for all groups when DMEM + 10% FBS was employed, suggesting protein corona formation and changes in the local dielectric environment of porphyrins, which modulate the optical properties.[29,30] However, no changes were detected within the red-laser range, indicating that the optical properties relevant to treatment efficacy were preserved. Importantly, the coating did not alter the intrinsic properties of the AuNPs, as particle hydrodynamic diameter at 0 h and cellular uptake remained unchanged for AuNP@TMPyP. On the other hand, in DMEM + 10% FBS at 24 h, a significant increase in the hydrodynamic diameter was identified for AuNPs whereas AuNPs@TMPyP exhibited a reduction in size. This decrease suggests a more homogeneous colloidal population in biological media. Such behaviour has been reported for photosensitizer-nanoparticle systems and may reflect dynamic interfacial effects rather than aggregation.[31] Nevertheless, the measured size remained within the range compatible with efficient cell internalization.[17]

LA-PEG$_{1k}$-COOH was chosen as coating to enhance colloidal stability, prevent aggregation, and enable covalent bond attachment of TMPyP through the carboxyl group.[32] On the other hand, the commercially available cationic porphyrin TMPyP was selected due to its quantum yield and demonstrated efficacy in oncological PDT, making it suitable for biological applications.[30] Indeed, upon laser exposure, TMPyP exhibited around 10% increase in $^1O_2$ production, whereas AuNPs@TMPyP achieved an increase of approximately 35%, suggesting that AuNPs presence enhanced $^1O_2$ generation, which produces strong local electromagnetic field enhancement by inducing collective oscillations of free electrons in subwavelength metallic nanoparticles, thereby increasing the effective light intensity.[33] Furthermore, the lack of increased $^1O_2$ under dual irradiation suggests no synergistic effect in this specific ROS production, potentially due to inefficient energy transfer mechanisms from gold to local oxygen or suboptimal activation

parameters, with levels resembling those observed for TMPyP under laser exposure.[34]

AuNPs have been shown to reduce TrxR activity following cellular internalization, which occurs predominantly via receptor-mediated endocytosis. After uptake, AuNP are trafficked to lysosomes, where the acidic environment promotes nanoparticle degradation and the release of gold ions. These ions subsequently inhibit TrxR through Au–thiol interactions at the enzyme active site, triggering oxidative stress, mitochondrial dysfunction, impaired DNA repair, and ultimately enhanced radiosensitization.[18] TrxR is a central component of the thioredoxin system, which is tightly interconnected with the peroxiredoxin and glutathione antioxidant systems through direct electron transfer reactions, shared dependence on NADPH, and compensatory detoxification of ROS, forming an integrated redox network rather than isolated pathways. Consequently, inhibition of TrxR is expected to have downstream effects on global redox homeostasis rather than representing a fully isolated or unique molecular event.[35] TrxR was selected as a molecular readout because it is a redox-active selenoenzyme that is highly sensitive to both gold-based materials and redox-active photosensitizers, and because cancer cells are known to rely strongly on the thioredoxin system to cope with elevated oxidative stress. Inhibition of TrxR therefore represents a strategic vulnerability within the broader redox network.

In addition, Penninckx et al. observed a strong correlation between AuNPs cellular uptake, TrxR residual activity and enhanced cell death for several cell lines, including MDA-MB-231, for which they obtained. An amplification factor at 2 Gy of $7 \pm 4\%$.[36] Our results are consistent with this finding, as we observed a reduction in TrxR activity alongside radiosensitizing effects. Specifically, AuNPs reduced TrxR activity by 40% compared to control cells, with an AF around 13% and 23% following X-rays and H^+ exposure, respectively. Notably, AuNPs@TMPyP induced a greater reduction in TrxR activity, showing a twofold decrease compared to AuNPs under the same conditions. Additionally, Prast–Nielsen and colleagues investigated the effects of porphyrins such as protoporphyrin IX and N-methyl protoporphyrin IX on TrxR inhibition in A549 cells. Their results demonstrated that porphyrins induce permanent inhibition of TrxR. In particular, protoporphyrin IX was shown to inhibit thioredoxin reductase 1 through a dual mechanism: acting as a competitive inhibitor of thioredoxin-1 at the C-terminal redox site while simultaneously promoting time-dependent, irreversible inactivation of the enzyme by targeting the redox-active selenocysteine residue, thereby disrupting electron transfer and impairing cellular redox homeostasis.[35] Thus, the individual inhibitory effects of AuNPs and TMPyP on TrxR, combined with their shared molecular mechanisms, suggest a complementary and potentially synergistic interaction when both components are associated in the AuNPs@TMPyP.

AF results further confirmed that AuNPs@TMPyP play a pivotal role under combined laser + IR compared to TMPyP free, showing an enhancement of approximately 15% for each radiation modality. Additionally, AuNPs@TMPyP exhibited significantly lower toxicity toward healthy cells in the laser + X-

rays modality. These features suggest that AuNPs@TMPyP could be a promising candidate for clinical translation. Indeed, MCF10A cells showed lower gold and TMPyP uptake than tumor cells. These findings align with literature that report that cancer cells internalize AuNPs more efficiently than healthy cells due to increased endocytic activity, altered membrane dynamics, and dysregulated intracellular trafficking associated with malignant transformation.[37]

Similarly, the preferential uptake of TMPyP by tumor cells can be attributed to the well-established behavior of cationic porphyrins in malignant tissues. Tumor cells typically display a more negatively charged plasma membrane, resulting from enhanced externalization of phosphatidylserine and increased expression of sulfated glycoproteins, which promotes strong electrostatic interactions with TMPyP. Moreover, malignant cells exhibit markedly elevated endocytic activity, further facilitating TMPyP internalization. Together, these intrinsic features of tumor cell biology provide a mechanistic basis for the higher porphyrin accumulation observed in cancer cells compared with non-tumorigenic MCF10A cells in the present study.[38]

Previous studies have shown that combination of RT with PDT is more effective than either modality alone.[15,16] Similarly, rice and colleagues reported a synergistic benefit of PDT combined with PT as salvage therapy for patients with malignant pleural mesothelioma.[39] However, AuNP@TMPyP-mediated PDT and IR, particularly involving charged particles, remains underexplored.

In this work, H^+ reduced the survival fraction by 40% compared to X-rays after 14 days. Indeed, the relative biological effectiveness (RBE) in our study was approximately 1.4, consistent with values reported in the literature for H^+ (Fig. SM1). Typically, protons RBE ranges around 1.1 at the tumor entrance to 1.15 in the center, and reach up to 1.35 at the distal edge, with values as high as 1.7 in the distal fall-off of the Bragg peak.[40] Additionally, LET is a key factor influencing RBE and the complexity extent of DNA damage. It is well-established that charged particles, such as H^+, induce more extensive DNA damage. In our study, the LET used for H^+ was 10 keV μm^{-1}, which is within the plateau region and is encompassed within the average used in clinic applications.

Our findings show that X-ray exposure significantly enhanced ROS generation in the control and AuNPs@TMPyP groups. In contrast, ROS levels from H^+ irradiation were lower than those observed after X-ray exposure. Interestingly, the AuNPs@TMPyP group exhibited an opposite trend under combined laser and IR modality: ROS levels were lower for laser + X-rays compared to X-rays alone, but higher for laser + H^+ compared to H^+ alone. This distinct behaviour may be attributed to differences in energy absorption and transfer mechanisms associated with each modality. Additionally, factors such as nanoparticle distribution, oxygen availability, the timing of ROS measurement, considering its rapid dynamic generation and propagation may contribute to these variations.[41]

It is also important to note that global ROS measurements may not fully capture the extent of biological damage induced by proton irradiation. In contrast to X-rays, which primarily exert their effects through indirect mechanisms involving water radiolysis and ROS generation, H^+ irradiation relies more strongly on direct energy deposition along the particle track, leading to more complex and clustered DNA damage.[8] Overall, these findings highlight that radiosensitization by AuNPs@TMPyP is not explained by the magnitude of global ROS generation, but rather sustained by redox imbalance resulting from TrxR inhibition and $^1O_2$ production.

According to our results, AuNPs@TMPyP disrupted $\Delta\Psi$ regardless of the radiation modality (laser, X-rays or H^+), as well as when laser was combined with IR. Consistently, AuNPs treatment reduced $\Delta\Psi$ in A549 cells 24 h after exposure and was accompanied by increased apoptotic levels. This effect is likely associated with elevated intracellular ROS production, which promotes cytochrome c release into the cytosol and activation of apoptotic pathways.[42] In parallel, red-laser irradiation has been shown to modulate cellular metabolism, primarily through mitochondrial pathways. Light-induced stimulation of the electron transport chain has been reported to alter mitochondrial function, redox balance and bioenergetic status, leading to changes in ROS signalling and $\Delta\Psi$. Rather than directly inducing DNA damage, these mitochondrial effects are thought to influence cellular stress responses and survival pathways, thereby modulating the cellular response to subsequent IR exposure and contributing to increased radiosensitivity.[43]

Apoptosis outcomes differed based on the radiation modality. The proportion of apoptotic cells was much higher after proton exposure compared to X-rays, regardless of the group (AuNPs, TMPyP, or AuNPs@TMPyP). Furthermore, AuNPs@TMPyP induced a higher percentage of late apoptosis/necrosis specifically under laser + X-rays/H^+. Overall, these findings provide insight into the effects of the multifaceted treatment at 24 h, which correlate with the reduced survival fraction observed 14 days post-treatments.

On the other hand, the analysis of spheroid viability on the last experimental day reveals distinct responses to each treatment modality. In the X-ray contexts, laser activation appears to convert AuNPs@TMPyP into effective radiosensitizers agent. Indeed, the laser + X-ray combination resulted in a significant reduction in spheroid viability, indicating a synergistic effect.

PT alone effectively suppressed spheroid viability, confirming its cytotoxic effect.[44] The combination of laser + H^+ did not further influence treatment outcome, as comparable effects were observed across the evaluated modalities. However, under the same treatment conditions, AuNPs@TMPyP exhibited greater efficacy than AuNPs or TMPyP.

Tudor *et al.* reported that in 3D chondrosarcoma spheroids, nanoparticle-assisted radiation therapy reduced cell survival, albeit less effectively than in 2D cultures, which was attributed to the limited penetration of nanoparticles within the spheroid structure.[45] In agreement with these findings, we observed a marked reduction in survival fraction in monolayer cultures exposed to AuNP@TMPyP-mediated PDT and IR, whereas 3D models exhibited a diminished response in the case of X-ray irradiation and no apparent sensitization under proton irradiation, highlighting the impact of 3D architecture on treatment efficacy. Accordingly, further studies are needed to optimize AuNPs and porphyrin concentrations, incubation protocols,

and cellular uptake specifically for 3D models, in order to better recapitulate the tumor microenvironment.

We propose an integrative model in which radiosensitization arises from the convergence of physical dose enhancement and redox imbalance. AuNPs contribute to radiosensitization by locally amplifying radiation-induced energy deposition and by inhibiting TrxR, thereby weakening a major cellular antioxidant defense. In parallel, TMPyP acts as a photosensitizer that promotes ROS generation upon light activation and, as supported by the literature, can also inhibit TrxR through competitive and redox-mediated mechanisms. The multimodal treatment therefore disrupts redox homeostasis at multiple levels, probably limiting the ability of cancer cells to detoxify radiation and PDT-induced oxidative stress.

Light penetration represents a constraint for PDT, particularly in deep-seated tumours; however, PDT may still be applicable in superficial lesions, intraoperative settings, or through the use of fiber-based or interstitial light delivery. The combination of laser-based PDT with proton therapy is technically challenging but increasingly feasible in specialized centers, and our work should be viewed as a proof-of-concept rather than a direct clinical protocol. Finally, we recognize the limitations inherent to *in vitro* models and emphasize that these findings require validation in more complex systems, such as *in vivo* models, to assess biodistribution, penetration, and therapeutic selectivity.

Conclusions

To our knowledge, this is the first study to combine AuNP-mediated PDT with IR in the context of TNBC, investigating the underlying mechanisms using AuNPs@TMPyP. Our findings show that AuNPs@TMPyP potentiate the dual-modality treatment by inhibiting TrxR, increased $^1O_2$ production, $\Delta\Psi$ disruption and enhanced selectivity toward cancer cells. Our data for 2D cultures demonstrate that AuNPs@TMPyP further enhanced the efficacy of combined PDT and X-rays in TNBC cells, as evidenced by a marked increase in the AF. In addition, PT showed greater efficacy than conventional RT in TNBC cells and yielded additional therapeutic benefits when combined with AuNPs@TMPyP and red laser. Nonetheless, due to the limited accessibility of PT, integrating X-ray-based RT with PDT mediated by AuNPs@TMPyP emerges as a promising and cost-effective alternative, with the potential to achieve comparable outcomes. Future work will be devoted to investigate the effects of AuNPs@TMPyP associated with different radiation modalities using an animal model.

Author contributions

Camila Ramos Silva – conceptualization, data curation, formal analysis, methodology, visualization and writing the original draft; Guillaume Berionni – methodology and data curation; Martha Simões Ribeiro – conceptualization, data curation, formal analysis, funding acquisition and writing-review; Anne-Catherine Heuskin – conceptualization, data curation, formal analysis, funding acquisition, supervision, writing-review and editing.

Conflicts of interest

There are no conflicts to declare.

Data availability

Acknowledgements

References

1 S. Al-Mahmood, J. Sapiezynski, O. B. Garbuzenko and T. Minko, Metastatic and triple-negative breast cancer: challenges and treatment options, *Drug Delivery Transl. Res.*, 2018, **8**(5), 1483–1507.

2 G. Bianchini, J. M. Balko, I. A. Mayer, M. E. Sanders and L. Gianni, Triple-negative breast cancer: challenges and opportunities of a heterogeneous disease, *Nat. Rev. Clin. Oncol.*, 2016, **13**(11), 674–690.

3 O. Obidiro, G. Battogtokh and E. O. Akala, Triple Negative Breast Cancer Treatment Options and Limitations: Future Outlook, *Pharmaceutics*, 2023, **15**(7), 1796.

4 J. Sukumar, K. Gast, D. Quiroga, M. Lustberg and N. Williams, Triple-negative breast cancer: promising prognostic biomarkers currently in development, *Expert Rev. Anticancer Ther.*, 2021, **21**(2), 135–148.

5 T. Marinko, Pericardial disease after breast cancer radiotherapy, *Radiol. Oncol.*, 2018, **53**(1), 1–5.

6 R. Mohan and D. Grosshans, Proton therapy - Present and future, *Adv. Drug Delivery Rev.*, 2017, **109**, 26–44.

7 W. D. Newhauser and R. Zhang, The physics of proton therapy, *Phys. Med. Biol.*, 2015, **60**(8), R155–R209.

8 K. Ilicic, S. E. Combs and T. E. Schmid, New insights in the relative radiobiological effectiveness of proton irradiation, *Radiat. Oncol.*, 2018, **13**(1), 6.

9 F. Holt, J. Probert, S. C. Darby, J. S. Haviland, C. E. Coles, A. M. Kirby, *et al.*, Proton Beam Therapy for Early Breast Cancer: A Systematic Review and Meta-analysis of Clinical Outcomes, *Int. J. Radiat. Oncol., Biol., Phys.*, 2023, **117**(4), 869–882.

10 N. Lalani, S. Alqarni and R. B. Jimenez, The Potential of Proton Therapy for Locally Advanced Breast Cancer: Clinical and Technical Considerations, *Curr. Oncol.*, 2023, **30**(3), 2869–2878.

11 J. S. Loeffler and M. Durante, Charged particle therapy–optimization, challenges and future directions, *Nat. Rev. Clin. Oncol.*, 2013, **10**(7), 411–424.

12 J. Gustalik, D. Aebisher and D. Bartusik-Aebisher, Photodynamic therapy in breast cancer treatment, *J. Appl. Biomed.*, 2022, **20**(3), 98–105.

13 P. He, F. Zhang, B. Xu, Y. Wang, W. Pu, H. Wang, *et al.*, Research progress of potential factors influencing photodynamic therapy for gastrointestinal cancer, *Photodiagnosis Photodyn. Ther.*, 2023, **41**, 103271.

14 J. H. Correia, J. A. Rodrigues, S. Pimenta, T. Dong and Z. Yang, Photodynamic Therapy Review: Principles, Photosensitizers, Applications, and Future Directions, *Pharmaceutics*, 2021, **13**(9), 1332.

15 C. R. Silva, D. P. Vieira, A. Z. de Freitas and M. S. Ribeiro, Photodynamic therapy as a strategic ally in radiotherapy for triple-negative breast cancer: the importance of treatment order, *Breast Cancer Res. Treat.*, 2025, **210**(3), 687–697.

16 S. Mayahi, A. Neshasteh-Riz, M. Pornour, S. Eynali and A. Montazerabadi, Investigation of combined photodynamic and radiotherapy effects of gallium phthalocyanine chloride on MCF-7 breast cancer cells, *J. Biol. Inorg. Chem.*, 2020, **25**(1), 39–48.

17 Y. Chen, J. Yang, S. Fu and J. Wu, Gold Nanoparticles as Radiosensitizers in Cancer Radiotherapy, *Int. J. Nanomed.*, 2020, **15**, 9407–9430.

18 S. Penninckx, A. C. Heuskin, C. Michiels and S. Lucas, The role of thioredoxin reductase in gold nanoparticle radiosensitization effects, *Nanomedicine*, 2018, **13**(22), 2917–2937.

19 S. Penninckx, A. C. Heuskin, C. Michiels and S. Lucas, Gold Nanoparticles as a Potent Radiosensitizer: A Transdisciplinary Approach from Physics to Patient, *Cancers*, 2020, **12**(8), 2021.

20 P. García Calavia, G. Bruce, L. Pérez-García and D. A. Russell, Photosensitiser-gold nanoparticle conjugates for photodynamic therapy of cancer, *Photochem. Photobiol. Sci.*, 2018, **17**(11), 1534–1552.

21 E. Oh, K. Susumu, R. Goswami and H. Mattoussi, One-phase synthesis of water-soluble gold nanoparticles with control over size and surface functionalities, *Langmuir*, 2010, **26**(10), 7604–7613.

22 R. Dědic, V. Vyklický, A. Svoboda and J. Hála, Phosphorescence of singlet oxygen and 5,10,15,20-tetrakis(1-methyl-4-pyridinio)porphine: Time and spectral-resolved study, *J. Mol. Struct.*, 2009, **924–926**, 153–156.

23 K. U. Wagner, Know thy cells: commonly used triple-negative human breast cancer cell lines carry mutations in RAS and effectors, *Breast Cancer Res.*, 2022, **24**(1), 44.

24 S. Li, S. Bouchy, S. Penninckx, R. Marega, O. Fichera, B. Gallez, *et al.*, Antibody-functionalized gold nanoparticles as tumor-targeting radiosensitizers for proton therapy, *Nanomedicine*, 2019, **14**(3), 317–333.

25 A. C. Wéra, H. Riquier, A. C. Heuskin, C. Michiels and S. Lucas, In vitro irradiation station for broad beam radiobiological experiments, *Nucl. Instrum. Methods Phys. Res., Sect. B*, 2011, **269**(24), 3120–3124.

26 A. C. Heuskin, A. C. Wera, H. Riquier, C. Michiels and S. Lucas, Low-dose hypersensitivity and bystander effect are not mutually exclusive in A549 lung carcinoma cells after irradiation with charged particles, *Radiat. Res.*, 2013, **180**(5), 491–498.

27 A. C. Wéra, A. Lobbens, M. Stoyanov, S. Lucas and C. Michiels, Radiation-induced synthetic lethality: combination of poly(ADP-ribose) polymerase and RAD51 inhibitors to sensitize cells to proton irradiation, *Cell Cycle*, 2019, **18**(15), 1770–1783.

28 R.-X. Wang, J.-J. Fan, Y.-J. Fan, J.-P. Zhong, L. Wang, S.-G. Sun, *et al.*, Platinum nanoparticles on porphyrin functionalized graphene nanosheets as a superior catalyst for methanol electrooxidation, *Nanoscale*, 2014, **6**(24), 14999–15007.

29 G. Maiorano, S. Sabella, B. Sorce, V. Brunetti, M. A. Malvindi, R. Cingolani, *et al.*, Effects of cell culture media on the dynamic formation of protein-nanoparticle complexes and influence on the cellular response, *ACS Nano*, 2010, **4**(12), 7481–7491.

30 A. Garcia-Sampedro, A. Tabero, I. Mahamed and P. Acedo, Multimodal use of the porphyrin TMPyP: From cancer therapy to antimicrobial applications, *J. Porphyrins Phthalocyanines*, 2019, **23**(01n02), 11–27.

31 S. S. Lucky, K. C. Soo and Y. Zhang, Nanoparticles in photodynamic therapy, *Chem. Rev.*, 2015, **115**(4), 1990–2042.

32 S. S. Banerjee, N. Aher, R. Patil and J. Khandare, Poly(ethylene glycol)-Prodrug Conjugates: Concept, Design, and Applications, *J. Drug Delivery*, 2012, **2012**, 103973.

33 S. Farooq and R. E. de Araujo, Identifying high performance gold nanoshells for singlet oxygen generation enhancement, *Photodiagnosis Photodyn. Ther.*, 2021, **35**, 102466.

34 M. Misawa and J. Takahashi, Generation of reactive oxygen species induced by gold nanoparticles under x-ray and UV Irradiations, *Nanomedicine*, 2011, **7**(5), 604–614.

35 S. Prast-Nielsen, T. S. Dexheimer, L. Schultz, W. C. Stafford, Q. Cheng, J. Xu, *et al.*, Inhibition of thioredoxin reductase 1 by porphyrins and other small molecules identified by a high-throughput screening assay, *Free Radical Biol. Med.*, 2011, **50**(9), 1114–1123.

36 S. Penninckx, A. C. Heuskin, C. Michiels and S. Lucas, Thioredoxin Reductase Activity Predicts Gold Nanoparticle Radiosensitization Effect, *Nanomaterials*, 2019, **9**(2), 295.

37 D. Fan, Y. Cao, M. Cao, Y. Wang, Y. Cao and T. Gong, Nanomedicine in cancer therapy, *Signal Transduct. Targeted Ther.*, 2023, **8**(1), 293.

38 K. Nishida, T. Tojo, T. Kondo and M. Yuasa, Evaluation of the correlation between porphyrin accumulation in cancer cells and functional positions for application as a drug carrier, *Sci. Rep.*, 2021, **11**(1), 2046.

39 S. R. Rice, Y. R. Li, T. M. Busch, M. M. Kim, S. McNulty, A. Dimofte, *et al.*, A Novel Prospective Study Assessing the Combination of Photodynamic Therapy and Proton Radiation Therapy: Safety and Outcomes When Treating

Malignant Pleural Mesothelioma, *Photochem. Photobiol.*, 2019, **95**(1), 411–418.

40 H. Paganetti, Relative biological effectiveness (RBE) values for proton beam therapy. Variations as a function of biological endpoint, dose, and linear energy transfer, *Phys. Med. Biol.*, 2014, **59**(22), R419–R472.

41 S. Chenna, W. J. H. Koopman, J. H. M. Prehn and N. M. C. Connolly, Mechanisms and mathematical modeling of ROS production by the mitochondrial electron transport chain, *Am. J. Physiol. Cell Physiol.*, 2022, **323**(1), C69–c83.

42 V. Ramalingam, K. Varunkumar, V. Ravikumar and R. Rajaram, Target delivery of doxorubicin tethered with PVP stabilized gold nanoparticles for effective treatment of lung cancer, *Sci. Rep.*, 2018, **8**(1), 3815.

43 C. Durães, A. Tabosa, E. Santos, S. Jesus, V. H. Guimarães, L. Queiroz, *et al.*, The effect of photobiomodulation on the radiosensitivity of cancer cells: a literature review, *Laser Med. Sci.*, 2025, **40**(1), 210.

44 D. W. Lee, J. E. Kim, G. H. Lee, A. Son, H. C. Park, D. Oh, *et al.*, High-Throughput 3D Tumor Spheroid Array Platform for Evaluating Sensitivity of Proton-Drug Combinations, *Int. J. Mol. Sci.*, 2022, **23**(2), 587.

45 M. Tudor, R. C. Popescu, I. N. Irimescu, A. Rzyanina, N. Tarba, A. Dinischiotu, *et al.*, Enhancing Proton Radiosensitivity of Chondrosarcoma Using Nanoparticle-Based Drug Delivery Approaches: A Comparative Study of High- and Low-Energy Protons, *Int. J. Mol. Sci.*, 2024, **25**(21), 11481.